

# Vapor Lubrication for Reducing Water and Ice Adhesion on Poly(dimethylsiloxane) Brushes

Shuai Li, Youmin Hou, Michael Kappl, Werner Steffen, Jie Liu,\* and Hans-Jürgen Butt\*

**Fast removal of small water drops from surfaces is a challenging issue in heat transfer, water collection, or anti-icing. Poly(dimethylsiloxane) (PDMS) brushes show good prospects to reach this goal because of their low adhesion to liquids. To further reduce adhesion of water drops, here, the surface to the vapor of organic solvents such as toluene or n-hexane is exposed. In the presence of such vapors, water drops slide at lower tilt angle and move faster. This is mainly caused by the physisorption of vapor and swelling of the PDMS brushes, which serves as a lubricating layer. Enhanced by the toluene vapor lubrication, the limit departure volume of water drop on PDMS brushes decreases by one order of magnitude compared to that in air. As a result, the water harvesting efficiency in toluene vapor increases by 65%. Benefits of vapor lubrication are further demonstrated for de-icing: driven by gravity, frozen water drops slide down the vertical PDMS brush surface in the presence of vapor.**

## 1. Introduction

Facilitating the sliding of liquid drops from solid surfaces is critical to keep windows transparent, enhance heat and mass transfer efficiency,<sup>[1]</sup> or inhibit ice deposition.<sup>[2]</sup> Strategies of regulating morphology and chemistry of surfaces are developed to achieve low lateral adhesion of sessile drops on surfaces. By constructing micro- and/or nanoscale structures with coating of low-surface-energy chemicals, superhydrophobic surfaces exhibit low contact angle hysteresis for water.<sup>[3]</sup> Water drops placed on superhydrophobic surfaces trap an air layer underneath. In this state, called the Cassie state, drops ball up and assume an almost spherical shape. The real contact

area between the drop and such surface is much lower than the apparent contact area. However, the surfaces tend to fail to repel water under pressure or condensed water formed at high-humidity conditions because no Cassie state is formed.<sup>[4]</sup> An alternative is to infuse porous nanostructures with a second liquid, which is immiscible with the drop. Such lubricant-infused surfaces show low lateral adhesion for liquids with a broad range of surface tensions as well as solids.<sup>[2b,5]</sup> However, lubricant is depleted by gravitational drainage, evaporation or sliding drops, which leads to the loss of the surfaces' low-lateral-adhesion performance.<sup>[6]</sup> Consequently, in order to realize the surfaces with both low liquid adhesion and long-term serviceability, the stability of the lubricant layer is a critical problem needs to be overcome.<sup>[2a,6a,7]</sup>

An alternative of low-lateral-adhesion surfaces is to covalently attach flexible macromolecule brushes onto smooth substrate, e.g., poly(dimethylsiloxane) (PDMS) brushes. With a small barrier of internal rotation of the O-Si-O bond, PDMS backbone are highly flexible.<sup>[8]</sup> The PDMS chains with one free side and high mobility make the brush layer demonstrate a liquid-like lubrication effect. Since the other side is covalently linked to the substrate the brush is not depleted by the applied liquids. However, comparing to superhydrophobic surfaces and lubricant-infused surfaces, the PDMS brushes still show a higher lateral adhesion to drops.<sup>[9]</sup>

To reduce lateral adhesion of sessile drops one needs to reduce the contact angle hysteresis, which is the difference between the advancing  $\theta_a$  and the receding contact angles  $\theta_r$ . The force required to move a drop laterally is given by<sup>[10]</sup>

$$F_c = w\gamma_L k(\cos\theta_r - \cos\theta_a) \quad (1)$$

where  $w$  is the width of the contact area of the drop,  $\gamma_L$  is the surface tension of the liquid in the drop and  $k \approx 1$  is a geometrical factor, which depends on the shape of the drop. To achieve low sliding angles and reduce the gravitational force needed for drops to slide, the difference between advancing and receding contact angles should be as small as possible. The lateral adhesion of water on the PDMS brushes can be further reduced and slide velocities increased via tethering liquid by the layer.<sup>[11,12]</sup> However, it's still a challenge to realize a durable liquid-tethered layer on PDMS brushes.

Here, we developed a strategy to reduce the adhesion of drops to PDMS brushes by exposing the surface to an organic solvent vapor. The brushes physically adsorb the vapor

S. Li, Y. Hou, M. Kappl, W. Steffen, J. Liu, H.-J. Butt  
Max Planck Institute for Polymer Research  
Ackermannweg 10, 55128 Mainz, Germany  
E-mail: liuje123@iccas.ac.cn; butt@mpip-mainz.mpg.de

Y. Hou  
School of Power and Mechanical Engineering  
Wuhan University  
Wuhan 430072, China

J. Liu  
Key Laboratory of Green Printing  
Institute of Chemistry  
Chinese Academy of Sciences  
Beijing 100190, China

The ORCID identification number(s) for the author(s) of this article can be found under <https://doi.org/10.1002/adma.202203242>.

© 2022 The Authors. Advanced Materials published by Wiley-VCH GmbH. This is an open access article under the terms of the Creative Commons Attribution License, which permits use, distribution and reproduction in any medium, provided the original work is properly cited.

DOI: 10.1002/adma.202203242

molecules because of the free energy of mixing between PDMS and solvent.<sup>[13]</sup> Thus, the thickness of the brush layer increases, which we confirmed later using atomic force microscopy (AFM) measurements.<sup>[14]</sup> As a result, the brushes become more flexible and water drop on such surface presents a lower sliding angle. With lower lateral adhesion, we found further benefits of the surface in promoting smaller drop departure radius, higher water collection rate, water drop manipulation, and lower ice adhesion. Ice adhesion also serves as a model for clathrate adhesion. Clathrates are a major problem in the oil and gas industry because they tend to block pipelines. We strongly indicates that clathrates behave similar to pure ice with respect to adhesion.<sup>[15]</sup>

## 2. Results and Discussion

To synthesize PDMS brushes,<sup>[16]</sup> oxygen plasma treated silicon wafers were immersed in a dimethyldichlorosilane-toluene solution (0.3 M), where the toluene is saturated with water. After 30 min, the substrate was coated with PDMS brushes. X-ray photoelectron spectroscopy proved the successful grafting of PDMS brushes because of the existence of the  $-\text{O}-\text{Si}(\text{CH}_3)_2-\text{O}-$  ( $\approx 102.5$  eV) besides  $\text{SiO}_2$  ( $\approx 103.5$  eV) from silicon wafer (Figure S1, Supporting Information). As schematically shown in Figure 1a, PDMS brushes tend to demonstrate a state that, one side of the PDMS chains is covalently attached on the substrate

and the other side is free. As a result, the water sliding angle and contact angles on PDMS brushes do not change even after ultrasonically clean in toluene (Figure S2, Supporting Information). The surface indeed shows low contact angle hysteresis against various liquids with different surface tensions, e.g., ethanol, toluene, dimethyl sulfoxide, etc. (Figure S3, Supporting Information). The brush layer thickness (measurement details given below) was  $\approx 4$  nm with the surface roughness being lower than 1 nm (Figure S4, Supporting Information). The layer thickness increases proportional to the grafting density  $\Gamma$  and the molecular mass of the PDMS chains  $M_w$  according to  $L = \Gamma M_w / \rho$ ; here,  $\rho$  is the density of PDMS. Unfortunately, we cannot yet determine  $\Gamma$  and  $M_w$  independently. In air saturated with water (at  $20 \pm 2$  °C), the surface is hydrophobic (Figure 1b) with advancing and receding contact angles for water of  $\theta_{ACA} = 106^\circ \pm 1^\circ$  and  $\theta_{RCA} = 102^\circ \pm 1^\circ$ , respectively.

Then we exposed the PDMS brushes to nitrogen gas with saturated water (to reduce the evaporation of water drop) and saturated vapor (at  $20 \pm 2$  °C, atmospheric pressure) of organic liquids which are not miscible with water, e.g., toluene, n-hexane. The vapor molecules are adsorbed and dissolved in the PDMS brushes (schematic showing in Figure 1a). As a result of the physisorbed vapor molecules, the brushes swell. In addition, the advancing contact angle decreased to  $102^\circ \pm 1^\circ$ , while the receding contact angle ( $101^\circ \pm 1^\circ$ ) changed little (Figure 1b). The resulted contact angle hysteresis of water in the presence of vapor decreased to  $1^\circ$ , while it was  $4^\circ$  in air.

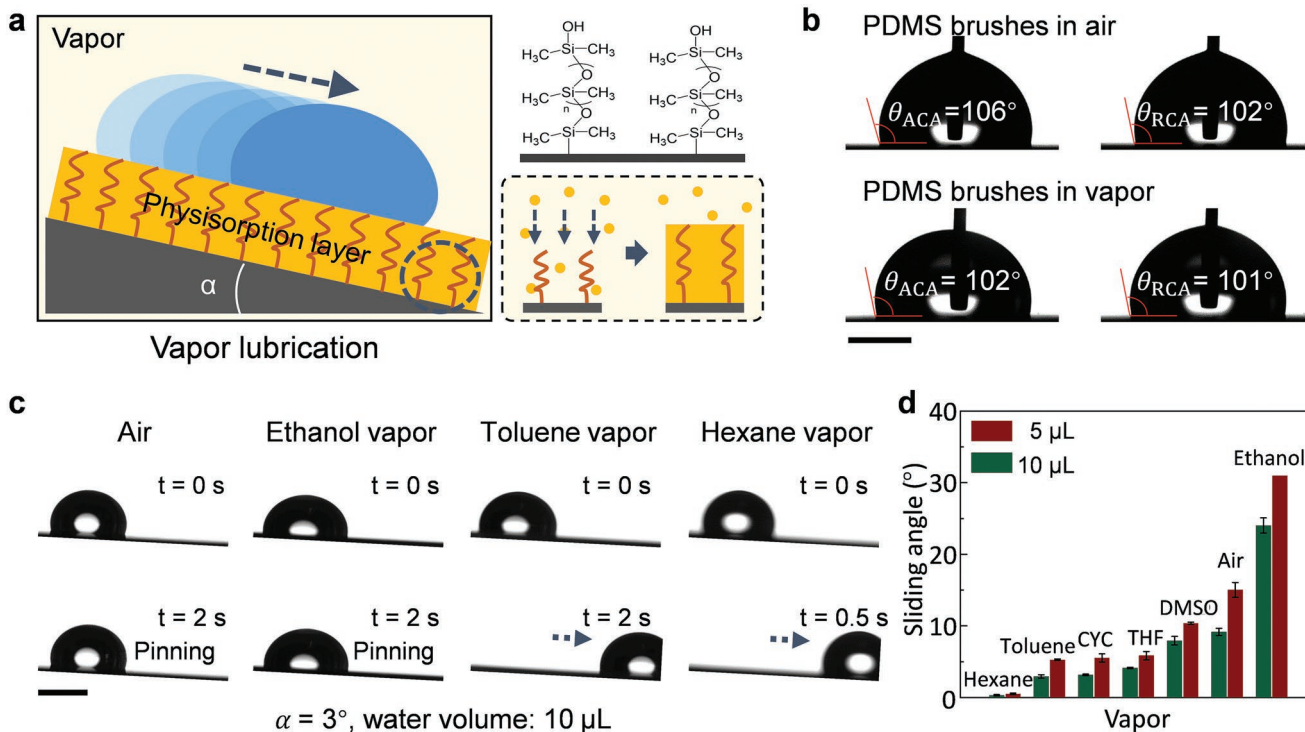


**Figure 1.** Vapor lubrication on PDMS brushes. a) Schematic of a water drop (blue) on a tilted surface which is coated with PDMS brushes (brown) in the presence of vapor (orange) and adsorbed lubricant layer. The adsorbed vapor leads to a swelling of the PDMS brushes.  $\alpha$  refers to the tilt angle of the surface. PDMS brushes are not drawn to scale. b) Advancing contact angle and receding contact angle of a water drop on PDMS brushes in air and vapor environment, respectively. Scale bar: 2 mm. c) Sliding of water drop (10  $\mu$ L) on a tilted PDMS brush surface ( $\alpha=3^\circ$ ) in air and saturated vapors of ethanol, toluene, and hexane. Scale bar: 2 mm. d) Sliding angles of water drops (5 and 10  $\mu$ L) on PDMS brushes in various vapors, e.g., hexane, toluene, cyclohexane (CYC), tetrahydrofuran (THF), dimethyl sulfoxide (DMSO), air, and ethanol. All data are presented in mean  $\pm$  standard deviations.

Furthermore, we found that the sliding ability of water drop is highly dependent on the applied vapor (Figure 1c). In the air and ethanol vapor, a water drop ( $10 \mu\text{L}$ ) pinned at a tilted angle  $\alpha = 3^\circ$ . In contrast, in the presence of toluene and n-hexane vapors, water drops start moving rapidly at this tilt angle. The vapor of hexane and toluene works as lubrication to accelerate the drop sliding.

To investigate the effect of different solvent vapor on the lubrication performance, we measured sliding angles of water drop with volume of 5 and  $10 \mu\text{L}$  in air and vapors of n-hexane, toluene, cyclohexane (CYC), tetrahydrofuran (THF), dimethyl sulfoxide (DMSO), and ethanol (Figure 1d). The presence of the vapor drastically changes the lateral adhesion of water drops. All vapors reduce the sliding angle, except for ethanol. The lubricating effect of the solvent vapor roughly correlates with the difference of solubility between solvent and PDMS (Figure S5, Supporting Information).<sup>[17]</sup> The lower the difference in solubility parameter, the lower the lateral adhesion of water drops. We speculate that the increase in contact angles hysteresis is also related to the miscibility of ethanol with water. The little amount of ethanol absorbed in the PDMS layer will be sucked up by the water drop. Thus, when the drop recedes it leaves behind a “dry” PDMS brush while at the front the PDMS brush still contains some ethanol and is still lubricated. The high contact angle hysteresis ( $\theta_{\text{CAH}} = 11^\circ \pm 1^\circ$ ) of water in ethanol vapor leads to an increase in the lateral adhesion (Figure S6, Supporting Information). According to Equation 1, the adhesion force of a  $10 \mu\text{L}$  water drop on PDMS brushes in ethanol

vapor is estimated to be  $49 \mu\text{N}$ , which is much higher than the value in air,  $11 \mu\text{N}$ . As a result, water drops show a bad mobility on PDMS brushes when in ethanol vapor. Moreover, on a low grafting density PDMS brushes, the vapor lubrication effect is also significant. The vapor lubrication decreased the water sliding angle from  $10^\circ$  to  $2^\circ$ , the contact angles hysteresis from  $7^\circ$  to  $1^\circ$  (Figure S7, Supporting Information).

To further investigate the lubricating effect of organic solvent vapors, we concentrate on toluene as a representative. We characterized the motion of water drops on tilted PDMS brushes in air, vapor, and with an added toluene drop (Figure 2a). Air or vapor saturated with water or water and toluene were utilized for inhibiting liquid evaporation. For the test of water sliding with an added toluene drop, a toluene drop was placed right next to a water drop on a horizontal PDMS-coated silicon wafer, the drops immediately coalesced followed by toluene forming a wetting ridge around the water drop.<sup>[18]</sup> The motions of  $10 \mu\text{L}$  water drops on tilted PDMS brushes at  $\alpha = 10^\circ$  in three environments (Figure 2b) show that: in air, water drops were pinned on the surface; once assisted by toluene, the water drops slide easily and rapidly on the surface. The reason is that the sliding angles (Figure 2c) decreased once toluene was introduced. For  $1 \mu\text{L}$  water drop as an example, the sliding angle on PDMS brushes in the presence of air, toluene vapor, and with a toluene drop were  $\approx 40^\circ$ ,  $\approx 12^\circ$ ,  $\approx 2^\circ$ , respectively. When increasing the volume of the toluene drop from 1 to  $10 \mu\text{L}$ , the sliding angle only showed a slight decrease from  $2^\circ$  to  $1^\circ$ , which is primarily caused by the increased volume of the coalesced drop.

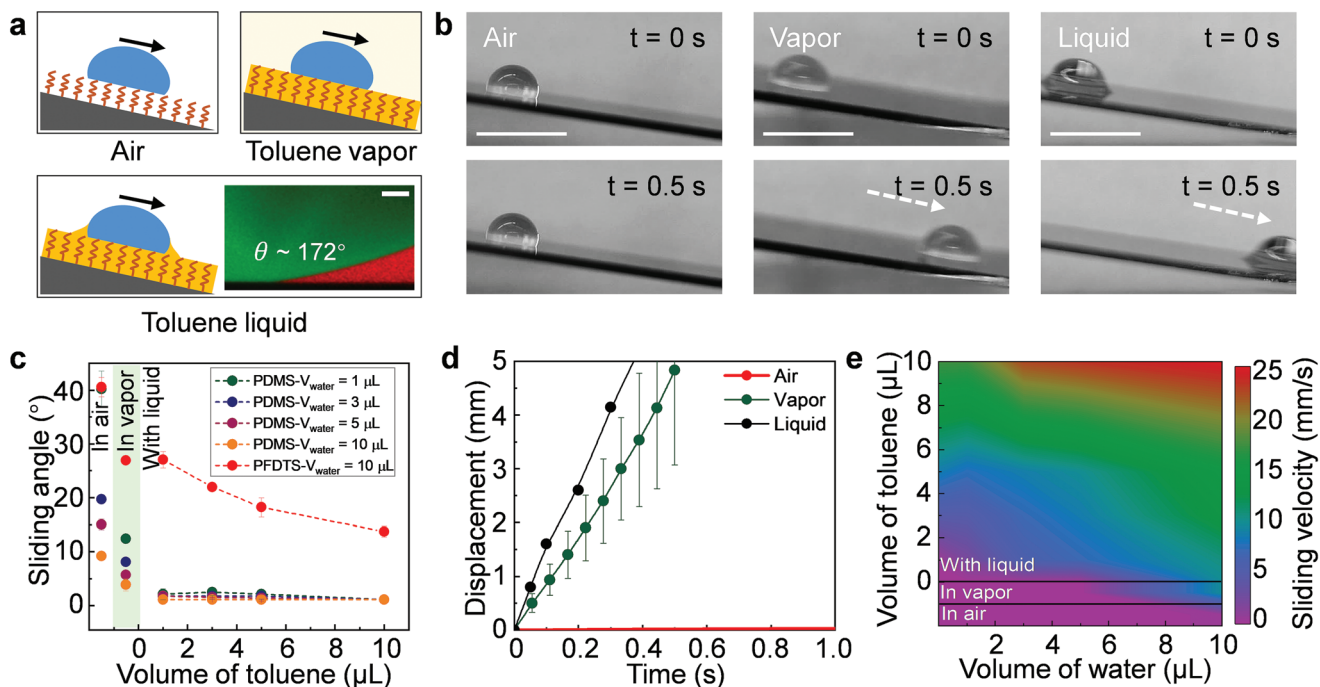


**Figure 2.** The sliding dynamics of the water drop on PDMS brushes in various conditions. a) Schematics illustrate the sliding characteristics of water drops on tilted PDMS brushes in air, vapor, and with an added toluene drop. PDMS brushes are not drawn to scale. Inset: Image taken by confocal microscopy showing the interface between water, toluene and the surface. b) Images showing the sliding of water drop ( $10 \mu\text{L}$ ) on the surface in three environments with  $\alpha = 10^\circ$ . Scale bar: 2 mm. c) Sliding angles of water drop ( $1, 3, 5$ , and  $10 \mu\text{L}$ ) on PDMS brushes in air, toluene vapor and with a toluene drop ( $1, 3, 5$ , and  $10 \mu\text{L}$ ). d) Displacement of a sliding water drop in different conditions. e) Velocities of water drop ( $V_{\text{water}} = 10 \mu\text{L}$ ) on PDMS brushes ( $\alpha = 10^\circ$ ) in three surroundings. The diagram was established based on the measured points. All data are presented in mean  $\pm$  standard deviations.

A vapor-induced change in sliding angle was also observed on other surfaces (Figure 2c). For example, on a wafer coated with PFDTs (1H, 1H, 2H, 2H-perfluorodecyltrimethoxysilane), the sliding angle for 10  $\mu\text{L}$  water drops was 40°. It decreased to 27° from air to saturated toluene vapor. The reduced effect is caused since a real lubricating layer is missing. With an added 10  $\mu\text{L}$  toluene drop on the PFDTs coated surface, the sliding angle of water decreased to  $\approx$ 14°.

The displacement ( $d$ ) of the water drops (10  $\mu\text{L}$ ) on PDMS brushes in toluene vapor and assisted by a toluene drop (3  $\mu\text{L}$ ) were very similar (Figure 2d). The displacement changes linearly with time ( $t$ ) in both cases, which is independent with the size of water drop (Figure S8, Supporting Information). The drops reached a steady state velocity within less than 0.1 s. The slopes reflect the sliding velocity of water drop, where  $v = d/t$ . Therefore, water drops sliding in toluene vapor has very closed velocity compared to that with a toluene drop. We systematically measured the sliding velocities of water drops of different volume on PDMS surfaces assisted by different amounts of toluene ( $V_{\text{toluene}}$ ) at tilt angles of  $\alpha = 10^\circ$  (Figure 2e). The water drops obtained higher mobility on PDMS brushes in toluene vapor when compared to that in air, especially in high water

volume region. The sliding velocity of water drop changes from 0.3 mm s $^{-1}$  in air to 10 mm s $^{-1}$  in toluene vapor and to 25 mm s $^{-1}$  when  $V_{\text{water}} = 10 \mu\text{L}$ . It suggests that vapor lubrication has reduced the lateral adhesion of water drops compared to that in air, even though it is still not as good as that assisted by toluene drops.

To verify the PDMS brushes can be swelled by the adsorbed vapor, we measured the brush thickness by atomic force microscopy (AFM). The thickness of PDMS brushes was deduced from force curves monitored during the tip approach (Figure 3a).<sup>[19]</sup> When the AFM tip gets into contact with the PDMS layer, it is wetted by the PDMS. As a result, capillary forces pull the tip towards the substrate until it contacts the hard substrate (Figure 3d). The same capillary attraction pulls the tip downwards in the presence of the toluene vapor. In this case the cantilever is bend so much that the spring force balances the capillary force (Figure 3b). For this reason the tip does not immediately jump into contact with the hard substrate. Once the tip is in contact with the hard substrate it follows the up-and-down movement of the sample stage of the AFM. We take the jump distance as a measure of the thickness of the brush layer. It is, however, only an estimate because of

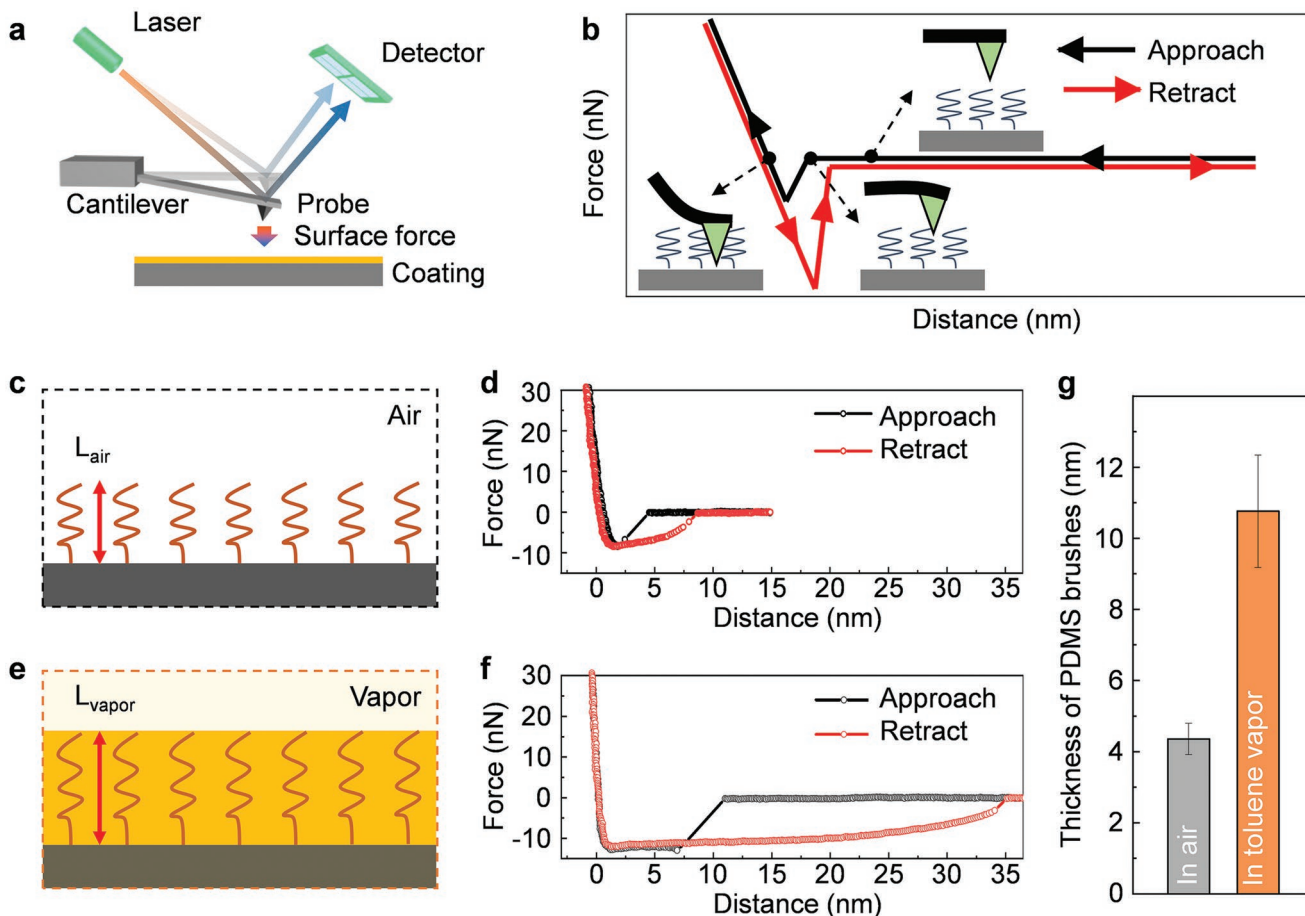


**Figure 3.** Characterization of the thickness of PDMS brushes. a) Schematic illustration of a AFM system for surface force measurement. b) Schematic illustrates the state of the AFM cantilever and tip corresponding to the force curve. c) Schematic image showing the state of PDMS brushes in air, and d) representative force curves measured by the AFM for PDMS brushes in air. PDMS brushes are not drawn to scale. e) Schematic image showing the state of PDMS brushes in toluene vapor, and f) representative force curves measured by the AFM for PDMS brushes in toluene vapor. g) The thickness of the PDMS brushes layer in air and toluene vapor. All data are presented in mean  $\pm$  standard deviations.

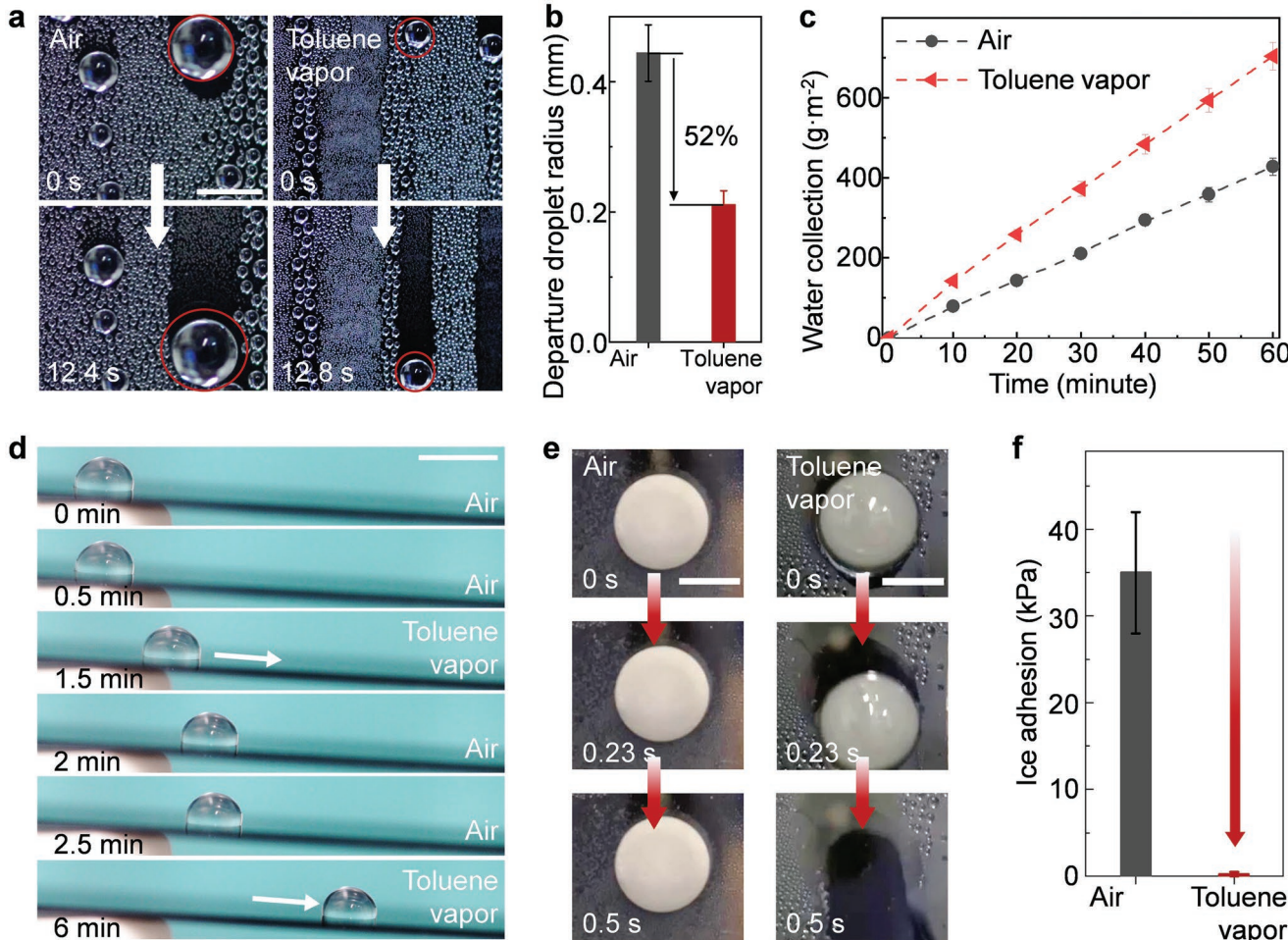


**Figure 4.** Applications of vapor lubrication. a) Photographs showing the departure of drops on PDMS brushes in air and toluene vapor. Scale bar: 1 mm. b) Departure size of condensed water on PDMS brushes in air and toluene vapor. c) The evolution of collected water during condensation with and without toluene vapor. d) Time-lapse photographs showing the controlled motions of water drop (20  $\mu$ L) on the tilted PDMS brushes ( $\alpha = 3^\circ$ ). Scale bar: 5 mm. e) Photographs showing the motion of an ice drop (150  $\mu$ L) on PDMS brushes in air and in toluene vapor environment. Scale bar: 5 mm. f) The lateral ice adhesion strength of a frozen water drop (50  $\mu$ L) on PDMS brushes in air and in toluene. All data are presented in mean  $\pm$  standard deviations.

two effects. First, the jump may occur slightly before the tip touches the brush surface because of van der Waals attraction. Second, since the PDMS chains are covalently attached to the Si wafer, some chains may still remain between tip and substrate even at a high force. While the first effect leads to a larger jump distance, the second effect reduces the jump distance.

When fully submerging the brush and tip in toluene, the tip gradually approached the substrate from a distance of 7.7 nm without a jump (Figure S9, Supporting Information). We did not detect a clear interface between toluene liquid and toluene-PDMS brushes mixture.

By comparing force curves in air and toluene vapor, we obtained direct evidence that the PDMS brush swells in toluene vapor and the layer thickness increases (Figure 3c-g). In air, the tip moves at a negative force over a few nanometers until it touches the substrate, indicating a PDMS brushes layer of several nanometers (Figure 3c,d). In toluene vapor, the tip undergoes a longer distance at negative force due to the swelling PDMS brushes layer (Figure 3e,f). After measuring

the thickness of PDMS brushes at 100 positions for each condition, average values of the brush thickness were obtained (Figure 3g; Figure S10, Supporting Information). The brush thickness changed from  $4.4 \pm 0.4$  nm in air to  $10.8 \pm 1.6$  nm in toluene vapor.

Accelerating drop departure from surfaces even for small drops is essential for enhancing liquid condensation and heat transfer.<sup>[1a-d,20]</sup> To test the condensation rate, we used a custom-built chamber (Figure S11a, Supporting Information) to cool the PDMS brushes at  $11 \pm 1$  °C. A stream of humid nitrogen gas (mass flow rate: 5 L  $\text{min}^{-1}$ ) with toluene vapor (details given in the Experimental Section) was input for condensation. Condensed water drops slid at a smaller size assisted by toluene on a vertical PDMS brushes (Figure 4a). As a result, the average drop departure radius in toluene vapor was  $0.21 \pm 0.02$  mm, which is less than half of that on PDMS brushes in air ( $0.44 \pm 0.04$  mm) (Figure 4b). A water harvest test shows that water collection efficiency in toluene vapor was improved (Figure 4c). According to the final size of condensed

droplets obtained from the video, we calculated the total volume of collected water by a spherical drop model and thus its mass. The linearly growing mass of collected water implies constant water harvesting rates for surfaces in both conditions. Compared with the case in air, the water collection rate in toluene vapor increased by  $\approx 65\%$ , which is  $\approx 700 \text{ g m}^{-2} \text{ h}^{-1}$ . It is the small departure drop radius in toluene vapor led to an early shedding of water drops from the surface and thus more room for newly condensing drops.

Vapor can also be used to control the motion of drops.<sup>[21]</sup> A 20  $\mu\text{L}$  water drop was placed onto a  $3^\circ$  tilted PDMS brushes surface (Figure 4d; Supporting Movie 1, Supporting Information). In air, it pinned without sliding ( $t < 1.5 \text{ min}$ ). When exposed to toluene vapor, the drop started to move on the surface ( $t = 1.5 \text{ min}$ ). After stopping the toluene vapor input, the water drop pinned again on the surface ( $t = 2 \text{ min}$ ). The sliding process can be repeatedly controlled by the appearance or disappearance of toluene vapor.

In addition to reducing the liquid lateral adhesion, toluene vapor also reduced ice adhesion to PDMS brushes (Figure 4e–g). The ice (50  $\mu\text{L}$ ) was formed after depositing a water drop on the PDMS brushes and cooling the surface. In air, the ice stickled to the surface even when turning it vertically without moving under its own weight. However, in the presence of toluene, the ice detached from the surface within 0.5 s. This decreased ice adhesion is mainly caused by the lubrication of the toluene vapor adsorbed by the PDMS brushes layer. The lateral ice adhesion strength was further quantified by a typical ice-adhesion characterization system (Figure S11b, Supporting Information).<sup>[2a,22]</sup> As shown in Figure 4g, the ice adhesion strength of  $35 \pm 7 \text{ kPa}$  was obtained on the surface in air. Once introducing toluene vapor, the adhesion strength decreased below 5 kPa. The absolute number of the adhesion force should not be overrated. Since the force transducer applies the force at a certain height, also vertical forces are exerted which may influence the result.

For practical applications, the strategy to use a vapor to form a lubricating layer is only applicable in closed chambers. Otherwise the vapor molecules which are adsorbed by the PDMS brushes would evaporate to the open environment. A possible application, where this condition is fulfilled is to coat the inside of pipelines with PDMS brushes coating. The aim is to prevent ice/hydrate formation and blocking of the pipeline. Natural gas consists of methane in addition to small amounts of other alkanes. Specifically, the methane inside the pipe would be adsorbed by the PDMS brushes and would act as a lubricant, thus the surface would be easier to repel ice. This is the similar case as we demonstrated here using toluene. Because of the low adhesion, the ice/hydrate would be easily removed by the moving fluid.

### 3. Conclusion

We have demonstrated how the lateral adhesion of water and ice to PDMS brushes can be reduced by the exposure to organic vapors. As confirmed by AFM, vapor molecules are adsorbed into the PDMS, swell the brushes and form a lubricating layer. Using vapor adsorption, the sliding angle for water drops can be reduced, and the slide velocity of water drops increases,

leading to its wide potential applications. With the departure volume of water drops being reduced by an order of magnitude with the assistance of toluene vapor, the water collection efficiency of condensing water drops was increased by  $\approx 65\%$  when compared to air. Furthermore, drop mobility can be manipulated by the presence of vapor. In the presence of organic vapor, the PDMS brushes show strong anti-icing properties by significantly reducing the lateral adhesion of ice. This provides a strategy to help solving the freezing-induced block of natural gas pipelines in winter.

### 4. Experimental Section

**Fabrication of PDMS Brushes and Fluorinated Surface:** The PDMS brushes were synthesized as described in the literature.<sup>[16]</sup> The silicon wafers (Silicon Materials Inc, P type,  $\langle 100 \rangle$  orientation) were washed in hexane (98%, Sigma) and ethanol (99.5%, Sigma) with ultrasonication for 5 min, respectively. Then the substrates were treated with an oxygen-plasma (Diener Electronic Femto, 120W,  $6 \text{ cm}^3 \text{ min}^{-1}$  oxygen flow rate) for 5 min. Afterwards, the substrates were immersed in 40 mL toluene (with saturated water) mixed with 1.4 mL dimethyldichlorosilane. After reacting for 0.5 h, the substrates were rinsed with toluene to remove the residues and dried with nitrogen. Glass cover slips (precision cover slips, Carl Roth GmbH + Co. KG, 24  $\times$  60  $\times$  0.17 mm) were coated in a similar way. The fluorinated surface was prepared as described in the following. The PDMS brushes by “grafting to” method is synthesized as following: A drop of silicon oil was deposited on the clean silicon surface, before put in the oven at 92 for 24 h. Afterwards, it was cleaned by hexane and water. The PFDTs was prepared as following: after oxygen plasma treatment as before, silica wafers were put into a vacuum desiccator with 20  $\mu\text{L}$  1H,1H,2H,2H-perfluorodecyltrimethoxysilane added in the bottom. Chemical vapor deposition was lasted for 12 h. Finally, the substrates were heated in an oven at 120 °C for 2 h.

**Contact Angles:** Advancing and receding contact angles were measured using a goniometer (OCA35, Dataphysics) when water volume was gradually ( $1 \mu\text{L s}^{-1}$ ) increased from 10 to 20  $\mu\text{L}$  and decreased from 10 to 20  $\mu\text{L}$ , respectively. The contact angles of water in toluene vapor were measured in a sealed chamber, in which toluene was used to generate saturated vapor. Each value was repeated for more than six times. All the experiments including the measurements below were conducted in atmospheric pressure without further statement.

**Sliding Angle:** The sliding angles were measured by the goniometer (OCA35, Dataphysics). A water drop (1, 3, 5, 10, 20  $\mu\text{L}$ ) was pipetted on the surface. Then the stage was started to rotate at a slow speed. The angle where the drop started to slide on the surface was recorded as sliding angle. Each result was repeated more than three times.

**Sliding Velocity:** The sliding velocity of water drops on PDMS brushes at a certain tilt angle was measured via analyzing the motion of the sliding drops recorded with a digital camera. For the test of water sliding with an added toluene drop, a toluene drop was placed right next to a water drop on a tilted PDMS-coated silicon wafer, the drops immediately coalesced followed by toluene forming a wetting ridge around the water drop. The motions of 10  $\mu\text{L}$  water drops on tilted PDMS brushes at  $\alpha = 5^\circ$  and  $10^\circ$  were recorded. The drop motions were then recorded for further analysis. Each result was repeated more than three times.

**Confocal Laser Scanning Microscopy:** A water drop (5  $\mu\text{L}$ ) and a toluene drop (5  $\mu\text{L}$ ) were deposited and allowed to coalesce on a glass surface coated by the PDMS brushes. The glass coverslip coated by PDMS brushes was mounted in the sample holder. The three phase contact area was observed with a confocal laser scanning microscope, Leica (Carl Zeiss, Jena, Germany) equipped with a C-Apochromat 40/1.2 W water-immersion objective. For excitation, two argon lasers fiber-coupled to the microscope were used (488 and 633 nm). Atto 488 and disperse blue 14 were used as dyes for water and toluene, respectively. Each measurement was conducted more than three times.

**AFM Measurements:** We used a Multi-Mode atomic force microscope (Bruker) in force spectroscopy mode to characterize the brush thickness in the air, in the presence of toluene vapor and liquid using a liquid cell. AFM silicon cantilevers (OLTESPA-R3 from Olympus) with a nominal spring constant of  $\approx 2$  N m $^{-1}$  and a nominal tip radius of 7 nm were used. The scan rate was 1 Hz and the scan range was set to 100 nm resulting in a scan speed of 100 nm s $^{-1}$ . Deflection sensitivity of the cantilevers was determined by taking cantilever deflection versus piezo position curves on a pristine silicon wafer before every experiment. Raw cantilever deflection (in detector voltage) versus piezo position data were recorded with a grid of 10 by 10 points on an area of  $0.5 \times 0.5 \mu\text{m}^2$ . These raw data were converted to force versus distance curves using the measured deflection sensitivity to obtain cantilever deflection in nanometers, multiplying cantilever deflection with the nominal spring constant to obtain force, and by subtracting cantilever deflection from piezo position to obtain distance.

**Condensation Measurements:** The departure size of drops and water harvesting performance were characterized from condensation experiments conducted in a custom-built device (Figure S11a, Supporting Information). Two separate vapor flows controlled by two mass flow controllers (FMA-A2208, Omega) were used to vary the concentration of toluene and water vapor inside a chamber. The vapors were obtained by bubbling nitrogen through water or toluene, respectively. The sample was fixed on a vertical copper block. The copper block was cooled by a Peltier element. Once condensed water drops reached a certain critical size, they slide off the surface driven by gravity.<sup>[1a,23]</sup> The subcooling was controlled at  $\approx 10$ K throughout the experiments. A Sony alpha 7R III camera was employed to record videos. Departure drop radius were calculated by comparing several time-lapse images before and after departure process. The volume of collected water was calculated by a sum of the sliding drops according to the videos.

**Ice Adhesion Measurements:** Anti-icing measurements were conducted in a custom-built chamber with cooling system (Figure S11, Supporting Information).<sup>[2a]</sup> A 50  $\mu\text{L}$  water drop was deposited on the surface, then the surface was cooled down to  $-25^\circ\text{C}$  to freeze the water drop. The force was continually recorded by a force gauge (PCE-DFG N 200) when the ice was pushed slowly at a speed of 60  $\mu\text{m s}^{-1}$ . The lateral adhesion force corresponds to the force when the ice moved on the surface (Figure S12, Supporting Information). The ice adhesion strength is defined as the adhesion force divided by the contact area (diameter: 5 mm). Thus, ice adhesion strength is in Pa (Figure 4f).

## Supporting Information

Supporting Information is available from the Wiley Online Library or from the author.

## Acknowledgements

This project has received funding from the European Research Council (ERC) under the European Union's Horizon 2020 research and innovation programme (Advanced grant DyanMo, No 883631). S.L. thanks the financial support from the China Scholarship Council (CSC). The authors thank Anke Kaltbeitzel for the support of confocal microscope, Dr. Rüdiger Berger for the support of Multimode-AFM, Dr. William S. Y. Wong for the support of anti-icing experiments, and Leon Prädel for XPS measurements.

Open access funding enabled and organized by Projekt DEAL.

## Conflict of Interest

The authors declare no conflict of interest.

## Author Contributions

S.L., J.L., and H.-J.B. designed the research and experiments. S.L. and J.L. carried out the surface fabrication. S.L. and M.K. conducted the force spectroscopy experiments. S.L. and Y.H. designed the condensation chamber for applications. S.L., Y.H., J.L., W.S., and H.-J.B. wrote the manuscript. All authors have given approval to the final version of the manuscript.

## Data Availability Statement

The data that support the findings of this study are available from the corresponding author upon reasonable request.

## Keywords

anti-icing, poly(dimethylsiloxane) brushes, vapor lubrication, water adhesion, wetting

Received: April 11, 2022

Revised: June 16, 2022

Published online: July 20, 2022

- [1] a) X. Wang, J. Zeng, J. Li, X. Yu, Z. Wang, Y. Zhang, *J. Mater. Chem. A* **2021**, *9*, 1507; b) Y. Hou, M. Yu, X. Chen, Z. Wang, S. Yao, *ACS Nano* **2015**, *9*, 71; c) R. Wen, X. Ma, Y. Lee, R. Yang, *Joule* **2018**, *2*, 2307; d) H. J. Cho, D. J. Preston, Y. Zhu, E. N. Wang, *Nat. Rev. Mater.* **2016**, *2*, 16092; e) M. Donati, C. W. E. Lam, A. Milionis, C. S. Sharma, A. Tripathy, A. Zendeli, D. Poulikakos, *Adv. Mater. Interfaces* **2020**, *8*, 2001176.
- [2] a) W. S. Y. Wong, K. I. Hegner, V. Donadei, L. Hauer, A. Naga, D. Vollmer, *Nano Lett.* **2020**, *20*, 8508; b) T. S. Wong, S. H. Kang, S. K. Tang, E. J. Smythe, B. D. Hatton, A. Grinthal, J. Aizenberg, *Nature* **2011**, *477*, 443; c) J. Lv, Y. Song, L. Jiang, J. Wang, *ACS Nano* **2014**, *8*, 3152; d) P. Irajizad, M. Hasnain, N. Farokhnia, S. M. Sajadi, H. Ghasemi, *Nat. Commun.* **2016**, *7*, 13395.
- [3] a) E. Y. Bormashenko, *Wetting of Real Surfaces*, De Gruyter, Berlin, Germany **2018**; b) X. Li, J. Yang, K. Lv, P. Papadopoulos, J. Sun, D. Wang, Y. Zhao, L. Chen, D. Wang, Z. Wang, X. Deng, *Natl. Sci. Rev.* **2021**, *8*, nwaa153.
- [4] R. Enright, N. Miljkovic, A. Al-Obeidi, C. V. Thompson, E. N. Wang, *Langmuir* **2012**, *28*, 14424.
- [5] a) D. Quéré, *Rep. Prog. Phys.* **2005**, *68*, 2495; b) J. D. Smith, R. Dhiman, S. Anand, E. Reza-Garduno, R. E. Cohen, G. H. McKinley, K. K. Varanasi, *Soft Matter* **2013**, *9*, 1772.
- [6] a) P. Baumli, M. D'Acunzi, K. I. Hegner, A. Naga, W. S. Y. Wong, H. J. Butt, D. Vollmer, *Adv. Colloid Interface Sci.* **2021**, *287*, 102329; b) S. K. Laney, M. Michalska, T. Li, F. V. Ramirez, M. Portnoi, J. Oh, I. G. Thayne, I. P. Parkin, M. K. Tiwari, I. Papakonstantinou, *Langmuir* **2021**, *37*, 10071.
- [7] S. Adera, J. Alvarenga, A. V. Shneidman, C. T. Zhang, A. Davitt, J. Aizenberg, *ACS Nano* **2020**, *14*, 8024.
- [8] a) B. Deloche, M. Beltzung, J. Herz, *J. Phys., Lett.* **1982**, *43*, 763; b) S. Krushev, W. Paul, G. D. Smith, *Macromolecules* **2002**, *35*, 4198; c) G. Huang, Q. Li, L. Jiang, *J. Appl. Polym. Sci.* **2002**, *85*, 545.
- [9] D. Daniel, J. V. I. Timonen, R. Li, S. J. Velling, M. J. Kreder, A. Tetrel, J. Aizenberg, *Phys. Rev. Lett.* **2018**, *120*, 244503.
- [10] A. Buzágh, E. Wolfram, *Kolloid-Z.* **1958**, *157*, 50.
- [11] A. Eifert, D. Paulissen, S. N. Varanakkottu, T. Baier, S. Hardt, *Adv. Mater. Interfaces* **2014**, *1*, 1300138.
- [12] H. Liu, P. Zhang, M. Liu, S. Wang, L. Jiang, *Adv. Mater.* **2013**, *25*, 4477.

- [13] N. A. Neuburger, B. E. Eichinger, *Macromolecules* **1988**, *21*, 3060.
- [14] a) A. L. Barnette, D. B. Asay, D. Kim, B. D. Guyer, H. Lim, M. J. Janik, S. H. Kim, *Langmuir* **2009**, *25*, 13052; b) A. J. Barthel, S. H. Kim, *Langmuir* **2014**, *30*, 6469.
- [15] N. Nguyen, R. Berger, M. Kappl, H. J. Butt, *J. Phys. Chem. C* **2021**, *125*, 21293.
- [16] J. Liu, Y. Sun, X. Zhou, X. Li, M. Kappl, W. Steffen, H. J. Butt, *Adv. Mater.* **2021**, *33*, 2100237.
- [17] J. N. Lee, C. Park, G. M. Whitesides, *Anal. Chem.* **2003**, *75*, 6544.
- [18] a) M. N. Popescu, G. Oshanin, S. Dietrich, A. M. Cazabat, *J. Phys.: Condens. Matter* **2012**, *24*, 243102; b) M. K. Chaudhury, G. M. Whitesides, *Science* **1992**, *255*, 1230.
- [19] H.-J. Butt, B. Cappella, M. Kappl, *Surf. Sci. Rep.* **2005**, *59*, 1.
- [20] R. Wen, S. Xu, X. Ma, Y.-C. Lee, R. Yang, *Joule* **2018**, *2*, 269.
- [21] a) L. Zheng, H. Li, W. Huang, X. Lai, X. Zeng, *ACS Appl. Mater. Interfaces* **2021**, *13*, 36621; b) V. Nasirimarekani, F. Benito-Lopez, L. Basabe-Desmonts, *Adv. Funct. Mater.* **2021**, *31*, 2100178.
- [22] a) J. Chen, J. Liu, M. He, K. Li, D. Cui, Q. Zhang, X. Zeng, Y. Zhang, J. Wang, Y. Song, *Appl. Phys. Lett.* **2012**, *101*, 111603; b) A. J. Meuler, J. D. Smith, K. K. Varanasi, J. M. Mabry, G. H. McKinley, R. E. Cohen, *ACS Appl. Mater. Interfaces* **2010**, *2*, 3100; c) M. J. Kreder, J. Alvarenga, P. Kim, J. Aizenberg, *Nat. Rev. Mater.* **2016**, *1*, 15003.
- [23] R. Mukherjee, A. S. Berrier, K. R. Murphy, J. R. Vieitez, J. B. Boreyko, *Joule* **2019**, *3*, 1360.